RSC Advances

PAPER

View Article Online
View Journal | View Issue

Cite this: *RSC Adv.*, 2024, **14**, 7040

Exploring the sensing potential of Fe-decorated h-BN toward harmful gases: a DFT study

Muhammad Isa Khan, *[a] Muhammad Imtiaz Akber,[a] Muhammad Gul,[a] Noor ul ain,[b] Tahir Iqbal,[c] Saleh S. Alarfaji[d] and Abid Mahmood*[e]

Gas sensing technology has a broad impact on society, ranging from environmental and industrial safety to healthcare and everyday applications, contributing to a safer, healthier, and more sustainable world. We studied pure and Fe-decorated hexagonal boron nitride (h-BN) gas sensor for monitoring of carbon-based gases using density functional theory (DFT). The calculations utilized the Generalized Gradient Approximation with the Perdew–Burke–Ernzerhof (GGA-PBE) exchange-correlation functional. The novelty of our study lies in the investigation of the adsorption of harmful gases such as carbonyl sulfide, carbinol, carbimide, and carbonyl fluoride on both pure and Fe-decorated h-BN. The deviation in structural, electronic, and adsorption properties of h-BN due to Fe decoration has been studied along with the sensing ability to design said material towards carbon monoxide (CO), carbon dioxide (CO_2), carbonyl sulfide (COS), carbinol, (CH_4O), carbimide (CH_2N_2), and carbonyl fluoride (CF_2O) gases. Gases such as CO, COS, CH_2N_2, and CF_2O exhibited chemisorption, while CO_2, and CH_4O exhibited physisorption behavior. The introduction of Fe altered the semiconductor properties of h-BN and rendered it metallic. Enhanced electronic properties were observed due to a robust hybridization occurring between the d-orbitals of Fe-decorated BN and the gas molecules. The extended recovery periods observed for gases, aside from CO_2, indicate their adhesive interactions with Fe-decorated h-BN. The reduction in desorption duration as temperature rises allows Fe-decorated h-BN to function as a reversible gas sensor. This research opens up a novel pathway for the synthesis and advancement of cost-effective, environmentally friendly double-atom catalysts with high sensitivity for capturing and detecting molecules such as CO, COS, CH_2N_2, CO_2, CH_4O, and CF_2O.

Received 22nd November 2023
Accepted 8th February 2024

DOI: 10.1039/d3ra08013g

rsc.li/rsc-advances

1. Introduction

Gas sensing has garnered significant interest in the modern world's management of climate pollution due to its widespread application in industrial control, medical treatment, indoor air quality management, and various other domains. Scientists have started looking into alternative sensing materials in response to the increased demand for gas sensors that are particularly sensitive, specific, stable, reversible, and versatile.[1–5] In recent times, there has been a significant increase in the concentrations of harmful gases such as CO, CO_2, NO, NH_3, and SO_2 in the atmosphere.[6,7] In the context of gas-sensing applications, a wide range of structures with diverse sizes, including bulk materials, have undergone considerable advancements.[8] The remarkable electrical conductivity, minimal electrical interference, and substantial surface-to-volume ratio of two-dimensional (2D) materials have harvested considerable attention.[9] The groundbreaking discovery of graphene has sparked a substantial increase in researcher interest in 2D materials. However, due to its low sensitivity and zero band gap, graphene is not ideal for sensing applications.[10] Graphene, the initial elemental 2D structure to be synthesized, has been utilized for detecting hazardous gases such as CO, NO, NO_2, NH_3, and more.[11] Lately, methods like atom substitution, adsorption, and the fabrication of heterostructures have been utilized to enhance the magnetic and electrical characteristics of 2D materials. These advancements find applications across various domains, including gas sensing, rechargeable batteries, and spintronics.[12–17]

Researchers have identified hexagonal boron nitride (h-BN), which shares similarities with graphene, as a valuable material for gas-sensing applications. In comparison to graphene, h-BN offers superior structural, chemical, and enhanced optical

[a]*Department of Physics, Rahim Yar Khan Campus, The Islamia University of Bahawalpur, Bahawalpur, Pakistan. E-mail: Muhammad.isa@iub.edu.pk; imtiazakbar4561@gmail.com; mgul@cern.ch*

[b]*Institute of Physics, Bagdad-ul-Jadeed Campus, The Islamia University of Bahawalpur, Bahawalpur, Pakistan. E-mail: noorulain@iub.edu.pk*

[c]*Department of Physics, University of Gujrat, Gujrat 50700, Pakistan. E-mail: tahir.awan@uog.edu.pk*

[d]*Department of Chemistry, Faculty of Science, King Khalid University, P.O. Box 9004, Abha 61413, Saudia Arabia. E-mail: ssalarvagi@kku.edu.sa*

[e]*Department of Environmental Sciences, Government College University, Faisalabad, Pakistan. E-mail: imabid4u@gmail.com*

properties, in addition to possessing a wide band gap and impressive thermal stability.[18–20] It emerges as a viable material for gas detection due to its exceptional thermal stability and impressive thermal conductivity, particularly in challenging environmental conditions. Both through computational simulations and empirical observations, various gas molecules have been found to adsorb onto the surface of h-BN, including but not limited to NO_2, NO, NH_3, CO, CH_4, and H_2.[21,22] In our prior research, a monolayer of h-BN was computationally designed and employed as a substrate to enhance the mechanical, electronic, and thermal properties of borophene for use in lithium-ion batteries as well as for gas sensing applications.[23,24]

Zhu *et al.* created a lateral heterojunction model through the synthesis of h-BN-graphene, observing variations in the bandgap of graphene with changes in the proportion of h-BN. Furthermore, they established adsorption structures for HCN, CO, NH_3, and Cl_2, conducting energy band calculations separately for the h-BN and Graphene segments within the h-BN-graphene lateral heterojunctions. In another study, the adsorption behavior of various gas molecules, including H_2S, SO_2, NH_3, and NO_2, was investigated on a diboron dinitride monolayer with point defects.[25,26]

Various approaches were undertaken to investigate the potential applications of h-BN, including the introduction of Fe doping on BN to examine its role in enhancing CO oxidation activity,[27] a computational design was employed to create a bilayer of h-BN for the assessment of its gas-sensing capabilities towards gases like CO_2, NO_2, and SO_2.[28] Additionally, dopants such as silver, silicon, manganese, and cobalt have been introduced into h-BN to augment its capability to adsorb a wide range of harmful gases.[29–31] To date, there have been no documented instances of utilizing Fe decoration on h-BN for the detecting of harmful gases.

In this research, we explore the adsorption of harmful gases, which include CO, CO_2, COS, CH_4O, CH_2N_2, and CF_2O, on Fe-decorated h-BN with the aim of assessing their potential for gas sensing applications. We systematically studied the structural parameters, adsorption properties, charge transfer, electronic properties, and sensing performance of the said material. The findings from these result analyses indicate that Fe-decorated h-BN displays favorable attributes for applications in detecting noxious gases.

2. Computational details

All computations were performed utilizing the Linear Combination of Atomic Orbitals (LCAO) approach within the BAND module of the Amsterdam Density Functional (ADF) software.[32] In ADF-BAND, we employed Slater-type orbital basis functions, renowned for their precision in modeling electron interactions near the nucleus. In our calculations, we employed the TZP basis set, conducting all-electron calculations without any core orbital restrictions.[33,34] The structural geometry was optimized without imposing any constraints. The calculations utilized the Generalized Gradient Approximation with the Perdew–Burke–Ernzerhof (GGA-PBE) exchange-correlation functional.[35]

The Kohn–Sham equations were solved for both the hexagonal lattice unit cell and the supercell of h-BN. The structural optimization utilized the quasi-Newton optimization method, specifically designed for handling delocalized modes when updating coordinates. Input files and parameters were configured through the graphical user interface (GUI) of the BAND code. BAND allows for the selection of periodicity/dimensions (1D for chains, 2D for slabs, and 3D for bulk) to implement periodic boundary conditions. Starting with the hexagonal unit cell of h-BN, simulations were conducted in both bulk and slab periodicities to investigate the material's 2D properties. Various electronic properties were examined using different parameters. Single point (SP) calculations were employed to compute nuclear gradients and derivatives of the Hessian for the optimized geometry, enabling the assessment of electronic properties.[32,34,36,37] We employed the D3-Grimme correction (DFT-D3) to account for van der Waals (vdW) effects, thereby enhancing the accuracy of the representation of long-range interactions between gas molecules and Fe-decorated h-BN.[38] The convergence criteria were set as energy (10^{-5} eV), gradient (0.02 eV $Å^{-1}$), and step-convergence (10^{-3} Å) for all structure relaxation.

The following equation was employed to calculate the binding energy

$$E_b = E_{(Fe\text{–decorated BN})} - E_{BN} - E_{Fe} \quad (1)$$

where E_b is the binding energy, $E_{(Fe\text{–decorated BN})}$ is the energy of the Fe decorated h-BN, E_{BN} is the total energy of the pristine h-BN, and E_{Fe} is the total energy of the Fe metal.[39,40]

The following equation was utilized to calculate adsorption energy

$$E_{ads} = E_{(material+gas)} - (E_{material} + E_{gas}) \quad (2)$$

Here $E_{(material+gas)}$is the sum of the total energy of the gas on the Material, $E_{material}$ is the energy of the Fe-decorated h-BN, and E_{gas} is the total energy of a gas molecule.[17,39] Using the Hirshfeld charge analysis method, we computed the charge transfer between the gas molecules and Fe-decorated h-BN.

3. Results and discussion

3.1. Geometry exploration

In this context, we are discussing the optimal configuration of both the pure and Fe-decorated h-BN, as illustrated in Fig. 1a and b. We opted a $4 \times 4 \times 1$ cell configuration to construct h-BN, each B and N contained 12 atoms. The lattice parameters of pure h-BN are $a = 10.25$ Å and $b = 8.85$ Å. The band distance between B–N is 1.48 Å. The angle between B–N–B or N–B–N are found to be same as 120°. The average B–N bond lengths appear to remain consistent even after the adsorption of a Fe atom. These findings align well with the information found in the existing literature.[29,30]

There are four possible adsorption sites on h-BN: the hollow (H), top on the nitrogen site (N), top on the boron site (B) and between the boron and nitrogen atom as (Br). These adsorption sites for Fe atom are labelled in Fig. 1a. The hollow site

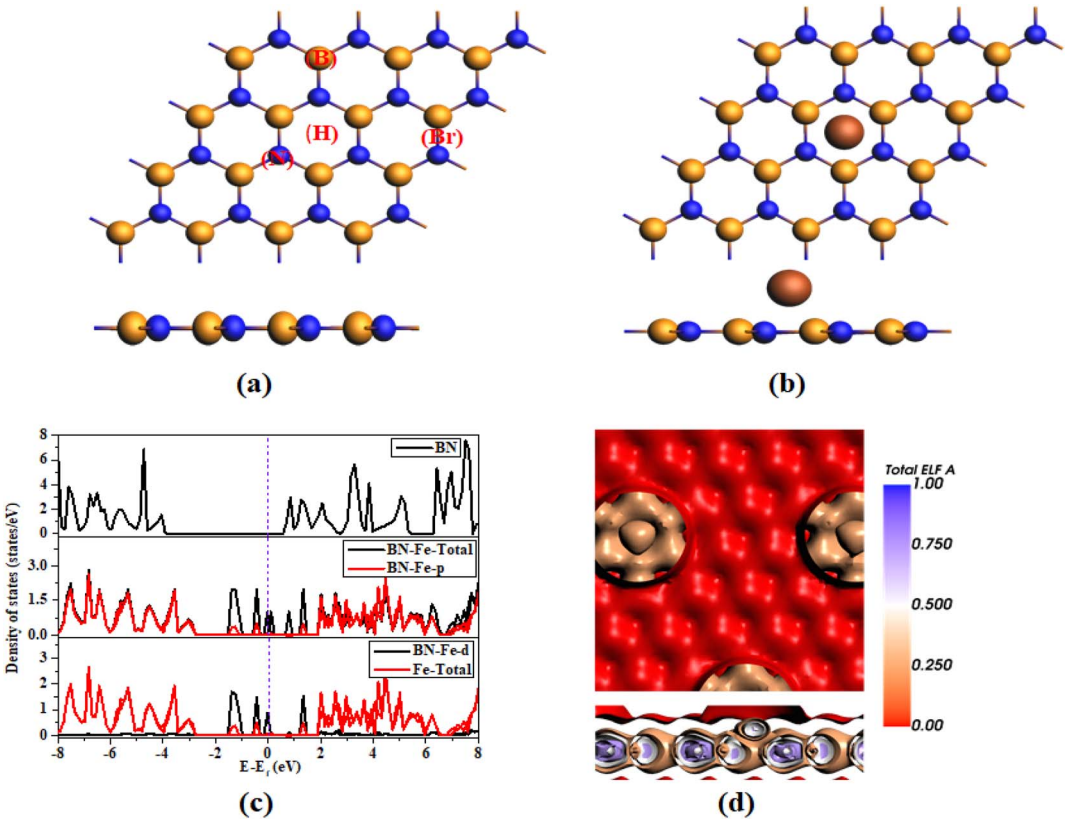

Fig. 1 Optimized geometry of (a) pure (b) Fe-decorated (c) DOS of pure and Fe-decorated h-BN (d) ELF map of Fe decorated h-BN.

appeared as preferable site due to its highest negative adsorption energy. The Fe decorated on the H site of the -BN has binding energy of −4.07 eV. The negative binding energy value indicates that the adsorption of Fe on h-BN is thermodynamically stable.

The Fig. 1c presents the DOS for both pure h-BN and Fe-decorated h-BN. The Fig. 1c shows the semiconducting behavior of h-BN with band gap of (4.5 eV) and after the adsorption of Fe on h-BN its behavior changes from semiconductor to metallic. The total DOS for the Fe-decorated h-BN monolayer exhibits a noticeable leftward shift when compared to the TDOS of the pure h-BN, indicating a transition to lower energy levels. Simultaneously, there is an overlap between the valence and conduction bands. This overlap contributes to the metallic bonding and allows electrons to move easily between energy states, resulting in a substantially higher electron distribution compared to the pristine h-BN monolayer. This suggests an enhancement in the substrate's conductivity following the introduction of Fe doping. These alterations demonstrate a shift in the system's behavior, there is a large number of available states at Fermi level for electrons to occupy. This contributes to the high conductivity of metallic materials. The contribution of the p-orbital to the DOS collectively forms both the valence band (VB) and conduction band (CB) in the system, as illustrated in Fig. 1c. The system's metallic behavior can be attributed to the presence of the d orbital within the system in combination with the total DOS of the Fe element. Additionally, the states of Fe significantly contribute to the formation of the VB and CB, as illustrated in Fig. 1c. These findings suggest a substantial alteration in the electronic structure of h-BN due to the incorporation of Fe. The resulting increased stability of the structure contributes to improving its gas-sensing performance. These results are consistent with the literature.[27,31]

3.2. The adsorption of gases on pure and Fe-decorated h-BN

In this section, we will explore the effectiveness of Fe-decorated h-BN in adsorbing gases such as CO, CO_2, COS, CH_4O, CH_2N_2 and CF_2O. To achieve highly stable adsorption arrangements, gas molecules are initially placed in different orientations in proximity to Fe-decorated h-BN. Fig. 2 illustrates optimized configurations after the adsorption of gases on Fe-decorated h-BN, displaying views from both the *x*-axis and *z*-axis perspectives. From the Fig. 2, it is evident that CO, COS, CH_2N_2, and CF_2O exhibit chemisorption behavior, whereas the others display physisorption. The carbon atoms of gases (CO, COS, and CH_2N_2), whereas the oxygen atom of the gas CF_2O, are attached to the Fe atom, confirming chemisorption behavior.

Table 1 presents the values for adsorption energy. The presence of negative values in the adsorption energy indicates that all the adsorption systems release energy, making them exothermic and facilitating spontaneous reactions. In case of pure h-BN the CF_2O exhibits highest adsorption energy while CO shows lowest. Regarding Fe-decorated h-BN, CF_2O gas displayed the highest adsorption energy at −7.2 eV, while CO_2

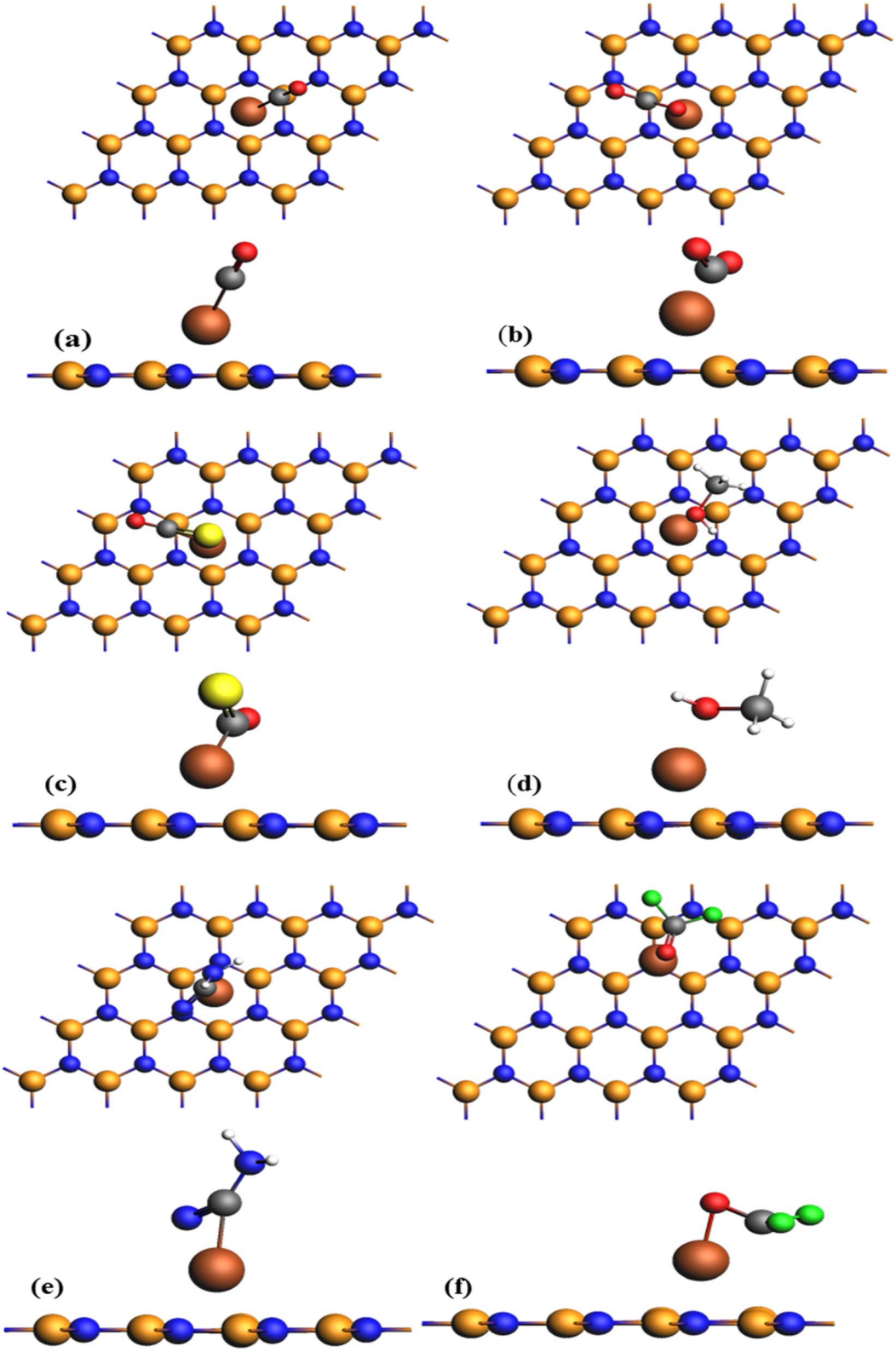

Fig. 2 Optimized structures of different gases such as (a) CO (b) CO_2 (c) COS (d) CH_4O (e) CH_2N_2 (f) CF_2O adsorbed on Fe-decorated h-BN.

exhibited the lowest at −1.42 eV. This also confirms the weak or physiosorption behavior of CO_2. The better adsorption energy (most negative) suggests that the adsorption of a gas on the material is more intensive and energetically favorable.[42–46] Therefore, Fe decoration enhanced the adsorption energy values than pure h-BN.

Table 1 Adsorption energy values of adsorbed gases on pure and Fe-decorated h-BN

Literature/gases (eV)	CO	CO_2	COS	CH_4O	CH_2N_2	CF_2O
Boron nitride (this work)	−1.28	−1.42	−1.78	−2.36	−3.47	−6.41
Fe-decorate h-BN (this work)	−5.79	−1.42	−2.89	−3.168	−4.47	−7.2
Fe-decorated antimonene[17]	−2.35	—	−2.31	—	—	—
Fe-doped Al[41]	−2.11	—	—	—	—	—

In our earlier investigation, antimonene was adorned with iron (Fe), and its gas sensing capabilities were explored. Various noxious gases, including CO, COS, NO, NO_2, NH_3, and SO_2, were adsorbed onto the Fe-decorated antimonene. The corresponding adsorption energy values were determined as −2.35 eV, −2.31 eV, −3.69 eV, −2.19 eV, −0.24 eV, and −1.54 eV. The elevated values of adsorption energy position this material as highly promising for applications in gas sensing.[17]

L.-Y. Guo *et al.* adsorb the silver (Ag) atom on pure h-BN to study the harmful gases such as NO NO_2, and SO_2F_2. They found the adsorption energy values as −0.817 eV, 1.893 eV, and −1.361 eV respectively. The adsorption of an Ag atom on BN exhibits a pronounced adsorption effect on gases, which can assist in discerning gas type, concentration, and production rate.[30] M. T. Ahmed *et al.* doped cobalt (Co) and manganese (Mn) on h-BN to study it for hazardous gases PH_3, NH_3, CH_4, O_3, H_2S, and SO_2. The doping of Co changed the behavior of h-BN to conductor while Mn changed it to semiconductor. The adsorption energy found negative for all the studied gases that confirms the exothermic behavior.[29]

Pandey *et al.* investigated the adsorption characteristics of three environmentally significant gases H_2, CO, and NO on both the pristine aluminene surface and the aluminene surface substituted with transition metal (TM) atoms. Interestingly, enhanced adsorption is observed for all gases on the TM-substituted aluminene compared to the pristine case. The recovery time results suggest that the adsorption of H_2 and CO gases on pristine aluminene, as well as H_2 gas on TM-functionalized aluminene surfaces, holds promise for use as a reusable gas sensor and for gas storage with subsequent facile release.[41]

In our prior study, we utilized computational methods to design interfaces involving borophene and boron nitride for the purpose of sensing industry-related gases, including CO, NO, CO_2, NH_3 and NO_2. The adsorption energy values for these gases are −2.7 eV, −1.8 eV, −3.7 eV, −3.4 eV and 4.0 eV.[24]

Nemati-Kande *et al.* studied the adsorption of different halomethanes such as CH_3F, CH_3Cl and CH_3Br on pristine, Al- and Ga-doped BN.[47] Esrafili *et al.* doped carbon on h-BN and studied its sensing properties for NO and NO_2 toxic gases. The inference drawn suggests that the adsorption of CO, CO_2, H_2O, or NH_3 on C-doped h-BN sheets is significantly less pronounced in comparison to NO and NO_2. The adsorption energy values decorated with C on B sites are −1.37 eV, −2.17 eV while on N site −1.77 eV and −2.49 eV.[48] This suggests that the adsorption of a Fe atom onto h-BN enhances the adsorption energies for all the gas systems studied.

3.3. Geometric analysis before and after gases adsorption

The significance of h-BN is indeed underscored by numerous studies focusing on its synthesis and characterization. For instance, Nicolosi *et al.* provided experimental validation of the hexagonal structure of boron nitride nanosheets, employing techniques like transmission electron microscopy (TEM), X-ray diffraction (XRD), and scanning electron microscopy (SEM). Wang *et al.*, in a separate investigation, presented experimental findings on the synthesis and characterization of graphene/h-BN heterostructures, which further affirmed the hexagonal lattice arrangement of boron nitride layers. Additionally, Kim *et al.* detailed experimental methodologies for the controlled synthesis of hexagonal boron nitride monolayers, complemented by geometric characterization utilizing atomic force microscopy (AFM) and high-resolution transmission electron microscopy (HRTEM). These studies collectively contribute to the extensive body of research supporting the understanding of h-BN and its properties.[49–52]

Fig. 2 illustrates the optimized arrangements of CO, CO_2, COS, CH_4O, CH_2N_2, and CF_2O molecules when adsorbed on Fe-decorated h-BN. The bond lengths of CO before optimization is (Fe–C) is 1.73 Å and (Fe–O) is 1.90 Å. After optimization, the bond length (Fe–C) increases to 1.77 Å and (Fe–O) is 2.94 Å. It displayed high chemisorption and interaction behavior. The COS gas molecule had the same behavior, with increase in bond length of (Fe–C) from 1.73 Å to 1.77 Å, and (Fe–O) bond length also increases from is 1.90 Å to 2.94 Å. A large change occurs in between the bind lengths of Fe and O. Due to low interaction with the Fe-decorated h-BN, CH_4O and CO_2 gas molecules showed physisorption behavior. The bond length before adsorption for CO_2 gas molecules is (Fe–O) is 2.54 Å and (Fe–C) is 2.22 Å, after absorption it increases to (Fe–O) is 3.02 Å and (Fe–C) is 1.93 Å. For gas CH_4O bond length (Fe–C) is 1.95 Å before adsorption, after adsorption band length (Fe–C) become 2.96 Å. The bond length before adsorption (Fe–C) is 1.44 Å and 1.57 Å for CH_2N_2 and CF_2O gas molecules, respectively, while it increases to (Fe–C) 1.87 Å and 1.93 Å.

The interactions between the mentioned gases indicate that Fe-decorated h-BN demonstrates chemisorption behavior with CO, COS, CH_2N_2, and CF_2O, while CH_4O and CO_2 exhibit physical adsorption.

3.4. Electronic properties analysis

The Density of States (DOS) distribution is of paramount importance for analyzing orbital interactions in each of the depicted adsorption systems in Fig. 3. It facilitates a more

profound understanding of the electronic analysis of gas and its adsorption on Fe-decorated h-BN.

Fig. 3 illustrates the d- and total DOS profiles of Fe, capturing the characteristics of the conduction and valence bands within the Fe-decorated h-BN. The adsorption of CO and carbinol gases did not alter the behavior of the Fe-decorated h-BN, while the other gases induced a shift in behavior towards a semi-conductor-like characteristic. Hybridization was identified among the DOS of the gas, Fe, and d states within the system at the Fermi level, serving as confirmation of the metallic behavior associated with the adsorption of CO and carbinol.

Prominent resonance peaks within the valence band, observed among the DOS of the gas, Fe, and d-states of the system, provide confirmation of the chemisorption behavior exhibited by CO, COS, CH_2N_2, and CF_2O gases. These peaks were detected within the energy ranges of (0 eV to −1 eV), (−0.4 eV to −2 eV), (−0.1 eV to −2.5 eV), and (−0.4 eV to −1.3 eV) for the gases CO, COS, CH_2N_2, and CF_2O, respectively. Furthermore, the DOS behavior of the Fe-decorated h-BN is inhibited by CO_2 gas, with no evidence of hybridization. This validates the physiosorption nature of the gas interaction with the material.

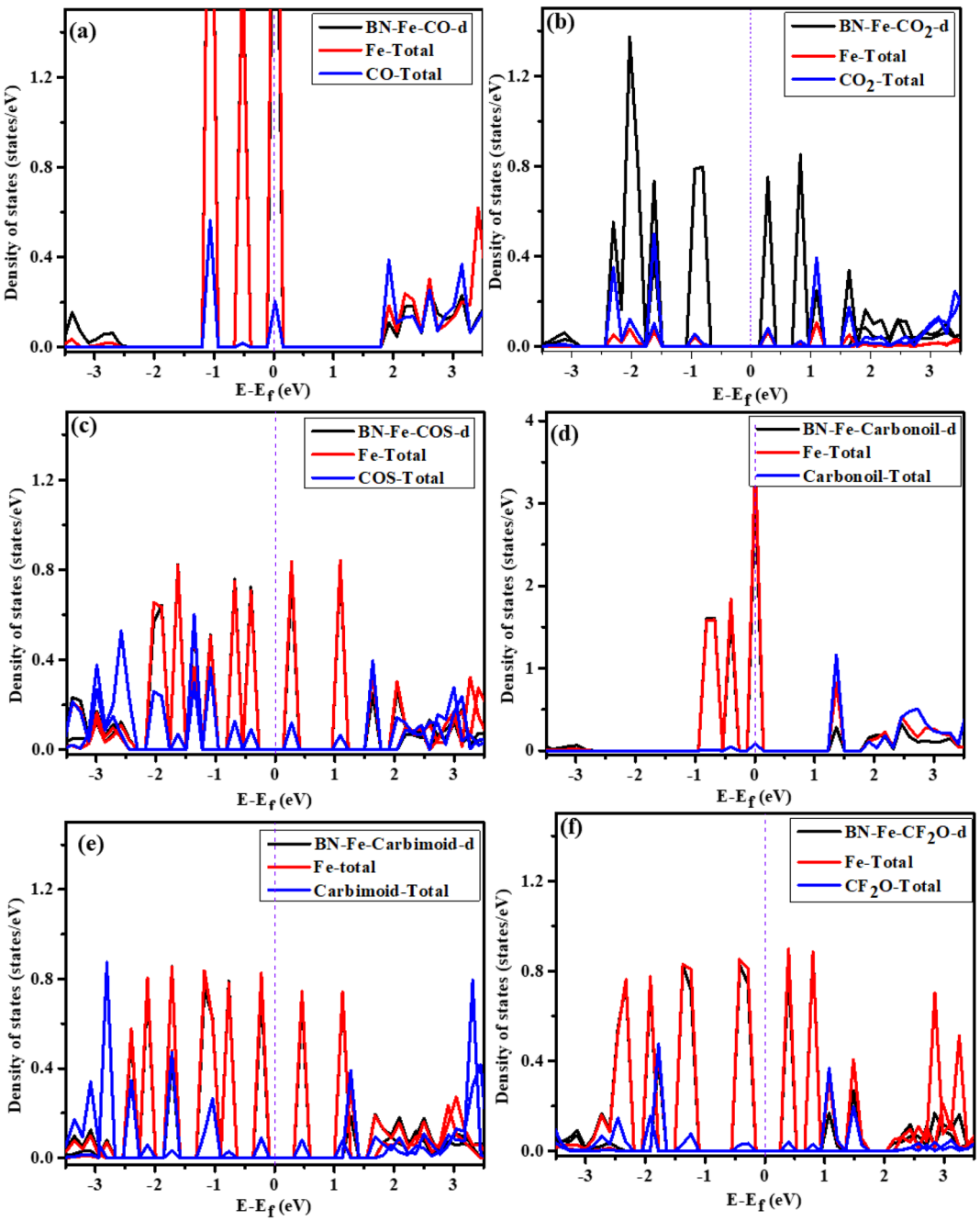

Fig. 3 Density of States of the adsorption of (a) CO (b) CO_2 (c) COS (d) CH_4O (e) CH_2N_2 (f) CF_2O gases on Fe-decorated h-BN.

In conclusion, the gases CO, COS, CH_2N_2, and CF_2O exhibit enhanced electrical properties due to their hybridization with Fe-decorated h-BN, and this correlation aligns well with the adsorption energy. In-addition, the analysis of gas adsorption for all these gases reveals noble metallic behavior, which is conducive to gas detection.

3.5. Charge investigation

We investigate interaction of gas molecules with the h-BN coated with Fe using Hirshfeld charge analysis. The introduction of Fe onto pure h-BN induces alterations in its electronic properties. While the initial band gap of pure h-BN is 4.5 eV, indicative of its semiconducting nature, this characteristic transforms into a metallic behavior upon Fe adsorption. The observed reduction in the band gap serves as compelling evidence for the substantial interaction between Fe metal and the h-BN surface. This interaction is primarily attributed to the electron-withdrawing effect exerted by the electron-rich nitrogen atoms of h-BN, causing a transfer of electronic density from Fe metal to h-BN. This charge transfer mechanism is responsible for the semiconductor-to-metal transition in the Fe/h-BN system, presenting it as a promising sensor for detecting the adsorption of specific hazardous molecules.[53]

Table 2 presents the charge values for systems with adsorbed gas on Fe-decorated h-BN. Evaluating the adsorption and detection of gases on the substrate can be assessed through charge analysis. The charge analysis shows that, on average, 0.209*e* charges are moved from the B atoms to the nearby N atoms because the N atom has a higher electronegativity, demonstrating that the pure BN's B–N bonds are somewhat ionic. Upon gas adsorption, boron and nitrogen atoms exhibit a partial negative and positive charge, respectively.

As electropositive elements, Fe displays the most substantial partial positive charges within the structure of Fe-decorated h-BN. Due to the attraction of electrons toward the electronegative elements in the adsorbed gas molecules; the partial positive charge of Fe became enhanced. Due to their electronegativity, the elements (N, O, S, and F) have partially negative charges, indicating that they are electron acceptors. The partially positive charges on the elements (B, Fe, and H) indicate that B, Fe, and H are electron donors.

In CH_4O, the C atom has a partially negative charge, whereas in CO, COS, CO_2, CH_2N_2, and CF_2O, it shows a partially positive charge. As a result, the C atom acts as an electron acceptor in the CH_4O molecule but an electron donor in the CO, COS, CO_2, CH_2N_2, and CF_2O molecules as shown in the Table 2. In CO and CO_2 gases, the carbon (C) atom transfers a charge of $-0.146e$ and $-0.185e$ to the oxygen (O) atom, respectively. Similarly, the O and S atoms in COS gas molecules develop charges of $-0.176e$ and $-0.071e$, correspondingly, due to charge transfer from C atoms.

3.6. Possibility of gas sensor

Usually, the adsorption of gases onto a host material results in changes in its electronic properties. The DOS results for Fe-decorated h-BN with adsorbed gases indicate alterations in the band gap due to gas adsorption. This alteration in the bandgap due to gas adsorption is a contributing factor to the changes in electrical conductivity. Let's examine the potential use of Fe-decorated h-BN as a gas sensor. Crucial factors such as sensitivity, stability, selectivity, and recovery, along with adsorption attributes like charge transfer and adsorption energy, are pivotal in modifying the DOS and enhancing electrical conductivity. These characteristics are essential for a material to function effectively as a reliable gas sensor.[54] When a gas molecule chemically bonds to the 2D sheets, resulting in a substantial E_{ads} value (indicative of chemisorption), it is usually accompanied by a significant exchange of charge and a reduction in the separation distance between the molecule and the sheet. Under such circumstances, the sheet has the potential to serve as a proficient gas sensor for the detection and sensing of gas molecules.[41] Therefore, the significant E_{ads} values suggest that gas molecules predominantly undergo chemisorption on both pure and Fe-decorated h-BN, except for a few instances like COS and CH_4O, which exhibit a preference for physisorption.

The evaluation of a gas sensor's sensitivity involves comparing the electrical conductivity (σ) of the systems before and after the adsorption of gas. The bandgap and temperature can be used to determine a material's electrical conductivity (σ) using the formula.[55–57]

$$\sigma = A \exp\left(\frac{-E_g}{2K_B T}\right) \quad (3)$$

Here, A is certain constant, T represents the temperature at 300 K; K_B stands for Boltzmann's constant, and E_g denotes the band

Table 2 Hirshfeld Charge distribution of pristine and gas-adsorbed Fe-decorated h-BN

Elements	BN (*e*)	Fe-BN (*e*)	Fe-BN + CO (*e*)	Fe-BN + CO_2 (*e*)	Fe-BN + COS (*e*)	Fe-BN + CH_4O (*e*)	Fe-BN + CH_2N_2 (*e*)	Fe-BN + CF_2O (*e*)
B	0.209	0.205	0.212	0.213	0.216	0.203	0.212	0.214
N	−0.209	−0.205	−0.207	−0.206	−0.206	−0.210	−0.207	−0.203
Fe	—	0.175	0.063	0.150	0.089	0.019	0.063	0.177
C	—	—	0.013	0.127	0.041	−0.019	0.005	0.159
O	—	—	−0.146	−0.185	−0.176	−0.111	—	−0.201
S	—	—	—	—	−0.071	—	—	—
H	—	—	—	—	—	0.059	0.130	—
N	—	—	—	—	—	—	−0.159	—
F	—	—	—	—	—	—	—	−0.092

Table 3 Electrical conductivity (σ) for the remarked gases at different temperatures

Gases	σ (Ω^{-1} m^{-1}) at $T = 300$ K	σ (Ω^{-1} m^{-1}) at $T = 600$ K	σ (Ω^{-1} m^{-1}) at $T = 900$ K
CO_2	4.97×10^{-9}	7.01×10^{-5}	1.7×10^{-3}
COS	1.2×10^{-5}	3.4×10^{-3}	2.2×10^{-2}
CH_2N_2	2.96×10^{-6}	1.71×10^{-3}	1.43×10^{-2}
CF_2O	2.15×10^{-7}	4.62×10^{-4}	5.97×10^{-3}

gap of the configurations. Table 3 shows the electrical conductivity at different temperature.

Our calculations show that the bandgap of Fe-decorated h-BN, adsorption of CO and CH_4O are 0 eV. Therefore, their conductivity becomes maximum. A slight shift in the bandgap causes an immediate change in electrical conductivity. After gas adsorption, the gas molecules CO, COS, CO_2, CH_4O, CH_2N_2 and CF_2O have different band gaps: such as (0 eV, 0.58 eV, 0.99 eV, 0 eV, 0.66 eV and 0.79 eV) respectively.

The conductivity of COS is greater as compare to other gases mentioned in the table because it has small band gap. With rising temperature, conductivity also experiences an increase. Table 3 reveals a direct relationship where conductivity increases as the temperature rises.

The formula for sensitivity (S)[58,59] is

$$\text{Sensitivity}, S = \left|\frac{\sigma_{\text{gas}} - \sigma_{\text{pure}}}{\sigma_{\text{pure}}}\right| \times 100\% \quad (4)$$

Here, σ_{gas} and σ_{pure} indicate to the electrical conductivity of the gas-adsorbed and pure systems, respectively. CO, and CH_4O, have 100% sensitivity whereas CO_2, COS, CH_2N_2 and CF_2O each have different. The bar chart in Fig. 4a illustrates that CF_2O exhibits the highest sensitivity, followed by COS, surpassing all other gases. Thus, all gas molecules show preferred detection on Fe-decorated h-BN surfaces. Selectivity is determined by dividing the most sensitive gas by all the other gases, as illustrated in the corresponding plot in Fig. 4b. CF_2O has sensitivity ratios of 1.05 to COS, 1.63 to CO_2, 1.24 to CO, 6.20 to CH_4O, and 11.27 to CH_2N_2 respectively. The results indicate that the sensor exclusively identifies CF_2O when it is present.

Apart from sensitivity, stability is another critical attribute of an effective gas sensor. If gas adsorption doesn't cause structural distortion, it is expected that the sheet will retain its stability. Therefore, it is reasonable to infer that the analyzed substrates remain stable when exposed to the gas adsorption under consideration.

We conducted a comparative analysis to measure the selectivity of these gases by calculating the ratios of the gas that exhibited the highest sensitivity to the others. In terms of a gas molecule's selectivity when interacting with a sheet, preference is given to the gas molecule with a higher observed E_{ads} over the one with a lower E_{ads}. Our adsorption energy results unequivocally show that CF_2O gas molecules exhibit the highest degree of adsorption on the analyzed surfaces, followed by CO, and then the other gases as outlined in Table 1.

Selectivity is evaluated by dividing the most sensitive gas by all the other gases, and you can see the corresponding chart in Fig. 4b. CF_2O exhibits sensitivity ratios of 1.63 to CO_2, 1.05 to COS, and 11.27 to CH_2N_2, respectively. The corresponding bar chart is displayed in Fig. 4b. These outcomes indicate that the sensor specifically identifies CF_2O in its presence. The selectivity among all gases becomes evident when compared to each other, primarily due to the substantial charge transfer between the gas and the surface, as well as a notable change in the electronic DOS following CO gas adsorption in contrast to the other two gas molecules.

3.6.1 Recovery time analysis. Evaluating sensors relies heavily on reusability, which typically represents the minimal duration necessary for a sensor to release adsorbed gases from its surface. To thoroughly assess the potential of Fe-decorated h-

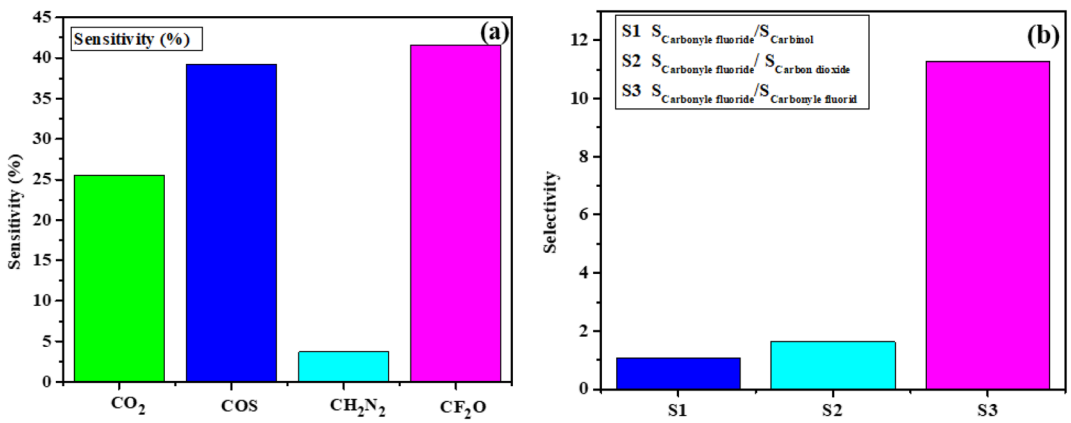

Fig. 4 (a) Sensitivity of the gas sensor based on Fe-decorated h-BN towards gas molecules, including carbon dioxide, carbonyl sulfide, carbimide, and carbonyl fluoride. (b) The selectivity of Fe-decorated h-BN sensor for carbonyl fluoride detection.

BN as a gas sensor, this section is dedicated to investigating the minimum desorption time required for six gases to detach from the surface of the sensing material, which is Fe-decorated h-BN. The recovery time measures the duration it takes for the gas to dissipate from the surface of the material, serving as a crucial metric for evaluating the detectability capability of sensing materials. The Van't Hoff–Arrhenius expression can be employed for the calculation of the recovery time in alignment with the principles of state theory.[60]

$$\tau = \nu_o^{-1} \exp\left(\frac{-E_{ads}}{K_B T}\right) \quad (5)$$

where K_B is the Boltzmann's constant (8.62×10^{-5} eV K^{-1}), T is the temperature, and frequency $\nu_o = 10^{12}$ s $^{-1}$.[16,61] In order to achieve reversible gas capture, the adsorption energies should fall within the range of −0.60 to −1.0 eV, respectively.[62] A greater E_{ads} would increase the challenge of gas desorption, but an increase in temperature would considerably expedite the process. The usability of the sensor relies on the recovery time values, which range from milliseconds to a few seconds. Nevertheless, an excessively brief recovery time implies inadequate adsorption capability, making it impractical for effective gas detection in the first place.[59] A more negative adsorption energy corresponds to an extended duration. Conversely, smaller values indicate reversible gas sensors. In this study, the recovery time is evaluated under conditions of visible light exposure and at different temperature. Table 1 displays the recovery times for all the examined gases computed at various temperatures.

Ahmed *et al.* employed first principles to explore the gas sensing application of cobalt- and manganese-doped boron nitride nanosheets. The calculated recovery time for the pristine material falls within the range of 10^{-12} s to 10^{-8} s, while the doping of Co and Mn increases it to 10^{38} s and 10^{41} s, respectively, attributed to higher adsorption energies.[29]

Xu *et al.* investigated the adsorption behaviors of H_2S, SO_2, NH_3, and NO_2 gas molecules on strategically defective diboron dinitride (n-BN) monolayers under various conditions, including the presence and absence of an external electric field and moisture. Recovery times for H_2S, NH_3, SO_2, and NO_2 on the n-BN monolayer were calculated at temperatures of 300 K, 473 K, 573 K, and 673 K. At 300 K, it is observed that H_2S, SO_2, and NO_2 exhibit prolonged recovery times, measuring 2.4×10^{14} s, 5.9×10^{43} s, and 1.6×10^{54} s, respectively, indicating challenges in desorption from the surface. Conversely, NH_3 demonstrates a shorter recovery time of 2.7 s at room temperature, showcasing its potential for efficient reuse in gas sensing and capturing applications.[25]

The greater recovery times for all gases at $T = 300$ K demonstrate their strong interaction with the Fe-decorated h-BN. In other words, the desorption of CO, CO_2, COS, CF_2O, and CH_4O gases from the surface is essentially impossible. For practical use, it is too difficult because the high gas recovery time of the Fe-decorated h-BN. The values of desorption time decrease, as the temperature rises as in Table 4. As a result, at high temperatures, the Fe-decorated h-BN behaves as a reversible gas sensor.

Therefore, the Fe-decorated h-BN sensor is ideal for gas sensing.

3.7. Electron localization function (ELF) analysis

The Electron Localization Function (ELF) serves as a valuable tool in quantum chemistry for scrutinizing electron distribution within a system, furnishing insights into the probability of locating an electron at a specific spatial point. ELF pertains to the kinetic energy density, serving as a metric for assessing both the concentration and dispersion of electrons.[63,64] The ELF ranges from 0.5 to 1.0, encompassing both bonding and nonbonding electron regions. Within this range, localized electron positions, such as those within a nucleus shell, covalent bonds, or a lone pair, are commonly observed. ELF values ranging from 0.0 to 0.5 signify weak van der Waals interactions, while electron delocalization occurs between electron shells.[65]

The colors discernible in the ELF map mirror these distinct electron density patterns. Within our investigation, these colors denote potential variations in electron density and bonding attributes. Fig. 1d displays the ELF of Fe-decorated h-BN. The red hue observed on the h-BN sheet and brown around the Fe atoms, hints at interactions between the metal atoms and the adjacent atoms in the h-BN sheet. These interactions encompass charge transfer between the Fe and h-BN.

ELF analysis also reveals regions of higher electron density. Fig. 5 illustrates the ELF images of gases adsorbed on Fe-decorated h-BN, displaying some variations in electron density for COS, CH_4O, and CH_2N_2 adsorbed on Fe-decorated h-BN. In contrast, CO, CO_2, and CF_2O adsorbed on Fe-decorated h-BN exhibit a consistent brown coloration around the gas, akin to Fe-decorated h-BN. However, there are observable pattern changes resulting from gas adsorption on Fe-decorated h-BN.

Table 4 Recovery time for the mentioned gases at different temperatures

Gases	τ (s) at $T = 300$ K	τ (s) at $T = 600$ K	τ (s) at $T = 900$ K	τ (s) at $T = 1200$ K
CO	2.50×10^{85}	4.98×10^{36}	2.92×10^{20}	2.23×10^{12}
COS	3.40×10^{36}	1.85×10^{12}	1.50×10^{4}	1.36
CO_2	7.03×10^{11}	8.39×10^{-1}	8.89×10^{-5}	1.60×10^{-7}
CH_4O	1.51×10^{41}	3.99×10^{14}	5.42×10^{5}	1.99×10^{1}
CH_2N_2	1.61×10^{63}	3.40×10^{25}	1.05×10^{13}	5.85×10^{6}
CF_2O	5.41×10^{108}	2.87×10^{48}	2.02×10^{28}	1.69×10^{18}

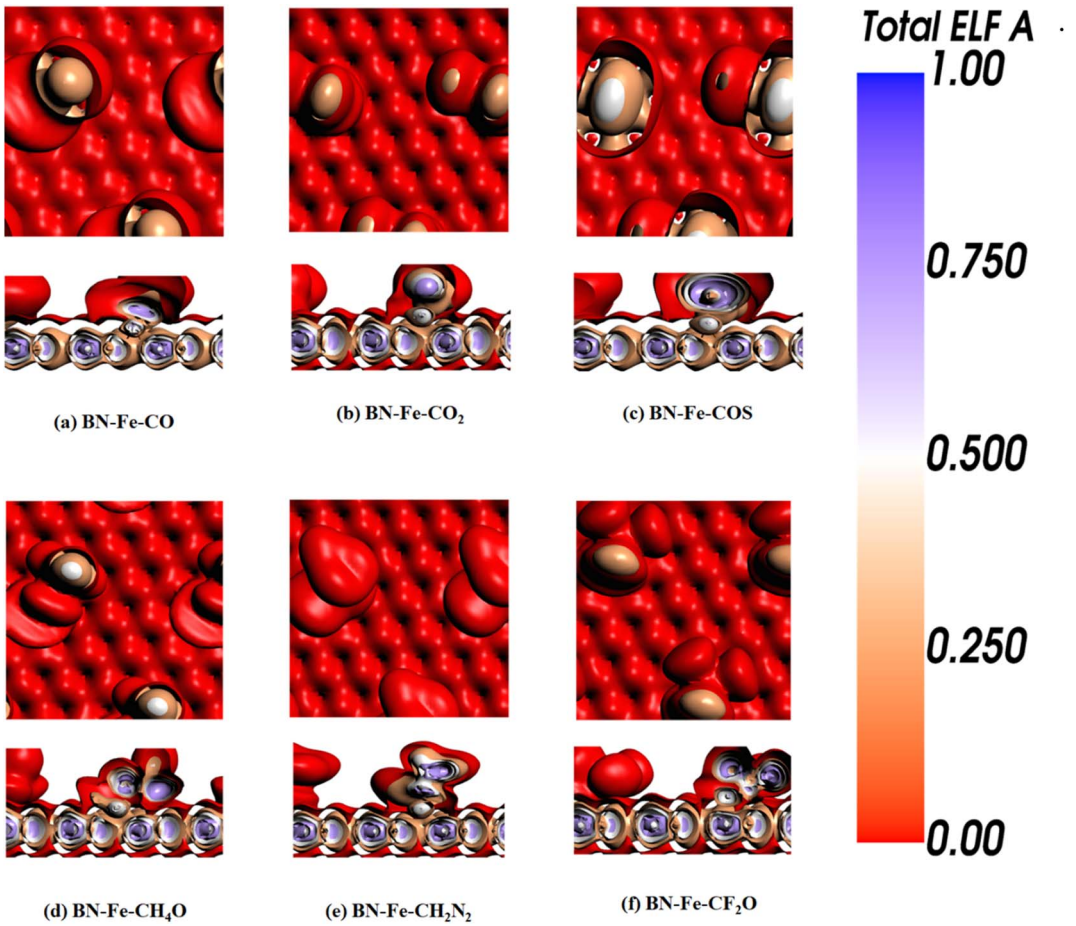

Fig. 5 ELF map of B_4C_3 monolayer adsorbed with 3d-TM. (a) BN–Fe–CO, (b) BN–Fe–CO_2, (c) BN–Fe–COS, (d) BN–Fe–CH_4O, (e) BN–Fe–CH_2N_2, (f) BN–Fe–CF_2O. The ELF values for the red, white, and blue colored sections are 0.00, 0.50, and 1.0, respectively.

4. Conclusions

We employed van der Waals dispersion-corrected Density Functional Theory (DFT) to investigate the adsorption of harmful gases, specifically CO, CO_2, COS, CH_4O, CH_2N_2, and CF_2O, on both pristine and Fe-decorated h-BN. The behavior of h-BN shifted from its semiconductor nature to a metallic state upon the adsorption of the Fe atom. The adsorption energy values experienced an increase upon the decoration of Fe on h-BN. Therefore, Fe-decorated h-BN is preferable than pure. CO_2 and CH_4O gases demonstrate physisorption, whereas CO, COS, CH_2N_2, and CF_2O gases exhibit chemisorption behavior. Among the gases, CF_2O had the highest adsorption energy, while CO_2 exhibited the lowest. The DOS results indicate that the adsorption of CO and CH_4O gases does not alter the conductive behavior of Fe-decorated h-BN. Performing accurate DFT calculations for systems involving gas molecules and surfaces can be computationally expensive, especially for large or complex systems. This may limit the size of the system that can be effectively studied. Involving of Basis Set Superposition Error (BSSE) corrections may improve the results. The sensitivity values for CO and CH_4O are both determined to be 100%, while the sensitivity for other substances varies. CF_2O has sensitivity ratios of 1.05 to COS, 1.63 to CO_2, 1.24 to CO, 6.20 to CH_4O, and 11.27 to CH_2N_2 respectively. Results show that the sensor only detects CF_2O when it is present. The extended recovery times for all gases at $T = 300$ K demonstrate their strong interaction with the Fe-decorated h-BN. ELF analysis are well agreed with the hirshfeld charge analysis. Moreover, the brown coloration indicates a concentrated electron density in regions where CO, CO_2, and CF_2O are adsorbed onto the h-BN sheet, suggesting the potential presence of covalent or polar covalent bonds involving carbon, oxygen, and fluorine atoms in CO, CO_2, and CF_2O with the h-BN sheet. Furthermore, at elevated temperatures, it might serve as a reversible gas sensor. These discoveries provide valuable theoretical insights for advancing the experimental design of innovative gas detection sensors incorporating Fe-decorated h-BN.

Conflicts of interest

The authors declare no conflict of interest.

Acknowledgements

The authors express their appreciation to the Deanship of Scientific Research at King Khalid University, Saudi Arabia, for

funding this work through research group program under grant number RGP. 2/445/44 to Saleh S Alarfaji.

References

1 A. Abbasi and J. Jahanbin Sardroodi, Structural and electronic properties of group-IV tin nanotubes and their effects on the adsorption of SO_2 molecules: insights from DFT computations, *J. Appl. Phys.*, 2018, **124**(16), 165302.
2 A. Abbasi and J. J. Sardroodi, An innovative gas sensor system designed from a sensitive nanostructured ZnO for the selective detection of SO_x molecules: a density functional theory study, *New J. Chem.*, 2017, **41**(21), 12569–12580.
3 A. Abbasi and J. J. Sardroodi, Exploration of sensing of nitrogen dioxide and ozone molecules using novel TiO_2/Stanene heterostructures employing DFT calculations, *Appl. Surf. Sci.*, 2018, **442**, 368–381.
4 C. Jin, *et al.*, A Janus MoSSe monolayer: a superior and strain-sensitive gas sensing material, *J. Mater. Chem. A*, 2019, **7**(3), 1099–1106.
5 X. Liu, *et al.*, A survey on gas sensing technology, *Sensors*, 2012, **12**(7), 9635–9665.
6 H.-Y. Li, *et al.*, Functional metal–organic frameworks as effective sensors of gases and volatile compounds, *Chem. Soc. Rev.*, 2020, **49**(17), 6364–6401.
7 S. M. Majhi, *et al.*, Recent advances in energy-saving chemiresistive gas sensors: A review, *Nano Energy*, 2021, **79**, 105369.
8 K. Patel, *et al.*, A new flatland buddy as toxic gas scavenger: A first principles study, *J. Hazard. Mater.*, 2018, **351**, 337–345.
9 S. S. Varghese, *et al.*, Two-dimensional materials for sensing: graphene and beyond, *Electronics*, 2015, **4**(3), 651–687.
10 A. C. Neto, *et al.*, AK Geim The electronic properties of graphene, *Rev. Mod. Phys.*, 2009, **81**(1), 109–162.
11 O. Leenaerts, B. Partoens and F. Peeters, Adsorption of H_2O, NH_3, CO, NO_2, and NO on graphene: A first-principles study, *Phys. Rev. B: Condens. Matter Mater. Phys.*, 2008, **77**(12), 125416.
12 I. khan Muhammad, K. Swera and M. Abdul, Computational study of 4d transition metals doped bismuthene for spintronics, *Phys. E*, 2021, **126**, 114464.
13 M. I. Khan, *et al.*, A DFT study of bismuthene as anode material for alkali-metal (Li/Na/K)-ion batteries, *Mater. Sci. Eng. B*, 2021, **266**, 115061.
14 M. I. Khan, *et al.*, Computational designing of Au-decorated buckled bismuthene and its application as a humidity gas sensor, *Mater. Chem. Phys.*, 2022, 127174.
15 M. I. Khan, *et al.*, Computational Studies of Super-B as Anodes for AM (Li, Na, and K) Ion Batteries, *J. Electrochem. Soc.*, 2022, **169**(9), 090514.
16 M. Isa, *et al.*, A DFT study of silver decorated bismuthene for gas sensing properties and effect of humidity, *Mater. Sci. Semicond. Process.*, 2022, **145**, 106635.
17 M. I. Khan, *et al.*, DFT perspective of gas sensing properties of Fe-decorated monolayer antimonene, *Appl. Surf. Sci.*, 2023, **616**, 156520.
18 D. Roy, *et al.*, Understanding the atomistic origin of the magnetic phases in Cobalt-TM (V, Nb, Ta, Zr, Hf, W) pair co-doped boron nitride monolayer and the hydrogenation effect, *Phys. E*, 2021, **125**, 114359.
19 M. T. Ahmed, S. Islam and F. Ahmed, Structural, optical, and electronic properties of boron nitride incorporated mobius carbon nanoribbon: a DFT calculation, *Phys. Scr.*, 2023, **98**(3), 035827.
20 S. Roy, *et al.*, Structure, properties and applications of two-dimensional hexagonal boron nitride, *Adv. Mater.*, 2021, **33**(44), 2101589.
21 A. A. Peyghan, *et al.*, A first-principles study of the adsorption behavior of CO on Al-and Ga-doped single-walled BN nanotubes, *Appl. Surf. Sci.*, 2013, **270**, 25–32.
22 A. Cadore, *et al.*, Enhancing the response of NH3 graphene-sensors by using devices with different graphene-substrate distances, *Sens. Actuators, B*, 2018, **266**, 438–446.
23 M. I. Khan, *et al.*, A DFT study on a borophene/boron nitride interface for its application as an electrode, *Phys. Chem. Chem. Phys.*, 2020, **22**(6), 3304–3313.
24 M. I. Khan, *et al.*, Computational study of borophene/boron nitride (B/BN) interface as a promising gas sensor for industrial affiliated gasses, *Phys. E*, 2021, **130**, 114692.
25 R. Xu, Z. Qiu and J. Guo, Theoretical evaluation of gas sensing and capturing characteristics on the point defective diboron dinitride monolayer, *J. Phys. Chem. Solids*, 2024, **184**, 111695.
26 P. Zhu, *et al.*, Electron regulation and gas-sensitivity analysis of hBN-Graphene lateral heterojunctions—First principle study, *J. Mol. Graphics Modell.*, 2024, **126**, 108658.
27 D. Li, W. Li and J. Zhang, Fe doped BN monolayer: A promising low-cost single atom catalyst for promoted CO oxidation activity, *Appl. Surf. Sci.*, 2020, **525**, 146567.
28 T. A. Hussein, *et al.*, Electronic and optical properties of the BN bilayer as gas sensor for CO_2, SO_2, and NO_2 molecules: A DFT study, *Results Chem.*, 2023, **5**, 100978.
29 M. T. Ahmed, *et al.*, First principles investigations of Cobalt and Manganese doped boron nitride nanosheet for gas sensing application, *Appl. Surf. Sci.*, 2023, **623**, 157083.
30 L.-Y. Guo, *et al.*, A DFT study of the Ag-doped h-BN monolayer for harmful gases (NO_2, SO_2F_2, and NO), *Surf. Interfaces*, 2022, **32**, 102113.
31 A. Yadav, Silicon-doped Boron Nitride Nanosheets for Enhanced Toxic Gas Sensing: An *ab initio* Approach, *Silicon*, 2023, **15**(4), 1847–1857.
32 G. T. Te Velde, *et al.*, Chemistry with ADF, *J. Comput. Chem.*, 2001, **22**(9), 931–967.
33 E. Van Lenthe and E. J. Baerends, Optimized Slater-type basis sets for the elements 1–118, *J. Comput. Chem.*, 2003, **24**(9), 1142–1156.
34 E. van Lenthe, E.-J. Baerends and J. G. Snijders, Relativistic total energy using regular approximations, *J. Chem. Phys.*, 1994, **101**(11), 9783–9792.
35 J. P. Perdew, K. Burke and M. Ernzerhof, Generalized gradient approximation made simple, *Phys. Rev. Lett.*, 1996, **77**(18), 3865.

36 A. D. Becke, Density-functional exchange-energy approximation with correct asymptotic behavior, *Phys. Rev. A*, 1988, **38**(6), 3098.
37 F. M. Bickelhaupt and E. J. Baerends, Kohn–Sham density functional theory: predicting and understanding chemistry, *Rev. Comput. Chem.*, 2000, 1–86.
38 S. Grimme, Semiempirical GGA-type density functional constructed with a long-range dispersion correction, *J. Comput. Chem.*, 2006, **27**(15), 1787–1799.
39 Y. Yu and C. Dai, DFT study of gas adsorption and sensing based on noble metal (Ag, Au and Pt) functionalized boron selenide nanosheets, *Phys. E*, 2021, **125**, 114409.
40 X. Wang and J. Wang, Effects of Pt and Au adsorption on the gas sensing performance of SnS2 monolayers: A DFT study, *Mater. Sci. Semicond. Process.*, 2021, **121**, 105416.
41 D. Pandey, *et al.*, Improved gas adsorption on functionalized aluminene surface: A first-principles study, *Appl. Surf. Sci.*, 2020, **531**, 147364.
42 V. Shukla, *et al.*, Toward the realization of 2D borophene based gas sensor, *J. Phys. Chem. C*, 2017, **121**(48), 26869–26876.
43 V. Nagarajan and R. Chandiramouli, Investigation on adsorption properties of CO and NO gas molecules on aluminene nanosheet: a density functional application, *Mater. Sci. Eng. B*, 2018, **229**, 193–200.
44 D. Cortés-Arriagada, N. Villegas-Escobar and D. E. Ortega, Fe-doped graphene nanosheet as an adsorption platform of harmful gas molecules (CO, CO_2, SO_2 and H_2S), and the co-adsorption in O_2 environments, *Appl. Surf. Sci.*, 2018, **427**, 227–236.
45 W. Xia, *et al.*, A first-principles study of gas adsorption on germanene, *Phys. Chem. Chem. Phys.*, 2014, **16**(41), 22495–22498.
46 M. Ashiq, *et al.*, Sensing applications of graphitic carbon nitride (g-C_3N_4) for sensing SO_2 and SO_3–A DFT study, *Phys. B*, 2024, 415661.
47 E. Nemati-Kande, M. Abbasi and M. D. Mohammadi, DFT studies on the interactions of pristine, Al and Ga-doped boron nitride nanosheets with CH3X (X= F, Cl and Br), *J. Mol. Struct.*, 2020, **1199**, 126962.
48 M. D. Esrafili and F. A. Rad, Carbon-doped boron nitride nanosheets as highly sensitive materials for detection of toxic NO and NO2 gases: a DFT study, *Vacuum*, 2019, **166**, 127–134.
49 J. Hassan, *et al.*, h-BN nanosheets doped with transition metals for environmental remediation; a DFT approach and molecular docking analysis, *Mater. Sci. Eng. B*, 2021, **272**, 115365.
50 V. Nicolosi, *et al.*, Liquid exfoliation of layered materials, *Science*, 2013, **340**(6139), 1226419.
51 L. Wang, *et al.*, One-dimensional electrical contact to a two-dimensional material, *Science*, 2013, **342**(6158), 614–617.
52 K. K. Kim, *et al.*, Synthesis of monolayer hexagonal boron nitride on Cu foil using chemical vapor deposition, *Nano Lett.*, 2012, **12**(1), 161–166.
53 M. Asif, *et al.*, Exploring the Sensing Potential of g-C_3N_4 *versus* Li/g-C_3N_4 Nanoflakes toward Hazardous Organic Volatiles: A DFT Simulation Study, *ACS Omega*, 2024, 3541–3553.
54 J. Zhang, *et al.*, Nanostructured materials for room-temperature gas sensors, *Adv. Mater.*, 2016, **28**(5), 795–831.
55 Y. Liu, *et al.*, Highly efficient VOC gas sensors based on Li-doped diamane, *Appl. Surf. Sci.*, 2023, **611**, 155694.
56 X. Zhang, *et al.*, Experimental sensing and density functional theory study of H2S and SOF2 adsorption on Au-modified graphene, *Advanced Science*, 2015, **2**(11), 1500101.
57 H. Cui, *et al.*, First-principles insight into Ni-doped InN monolayer as a noxious gases scavenger, *Appl. Surf. Sci.*, 2019, **494**, 859–866.
58 A. Aasi, S. Mehdi Aghaei and B. Panchapakesan, Outstanding performance of transition-metal-decorated single-layer graphene-like BC6N nanosheets for disease biomarker detection in human breath, *ACS Omega*, 2021, **6**(7), 4696–4707.
59 R. P. Reji, *et al.*, First-Principles Density Functional Theory Calculations on the Potential of Sc2CO2 MXene Nanosheets as a Dual-Mode Sensor for Detection of Volatile Organic Compounds in Exhaled Human Breath, *ACS Appl. Nano Mater.*, 2023, **6**(7), 5345–5356.
60 Y.-H. Zhang, *et al.*, Improving gas sensing properties of graphene by introducing dopants and defects: a first-principles study, *Nanotechnology*, 2009, **20**(18), 185504.
61 K. Yamaguchi, *et al.*, A spin correction procedure for unrestricted Hartree-Fock and Møller-Plesset wavefunctions for singlet diradicals and polyradicals, *Chem. Phys. Lett.*, 1988, **149**(5–6), 537–542.
62 S. Aghaei, *et al.*, Graphene-like BC6N nanosheets are potential candidates for detection of volatile organic compounds (VOCs) in human breath: A DFT study, *Appl. Surf. Sci.*, 2021, **536**, 147756.
63 B. Silvi and A. Savin, Classification of chemical bonds based on topological analysis of electron localization functions, *Nature*, 1994, **371**(6499), 683–686.
64 C. S. Abraham, *et al.*, Computational evaluation of the reactivity and pharmaceutical potential of an organic amine: A DFT, molecular dynamics simulations and molecular docking approach, *Spectrochim. Acta, Part A*, 2019, **222**, 117188.
65 M. Vatanparast and A.-R. Nekoei, RAHB concept and σ-skeleton in some oximes of 3-hydroxy fulvene; DFT, AIM, ELF and NBO studies, *Struct. Chem.*, 2015, **26**, 1039–1048.